

GENERATION OF EXPERIMENTAL DATA FOR MODEL TRAINING TO OPTIMIZE FOULING PREDICTION

*N. Jarmatz, W. Augustin and S. Scholl

Technische Universität Braunschweig, Institute for Chemical and Thermal Process Engineering,
Langer Kamp 7, 38106 Braunschweig, Germany
*n.jarmatz@tu-braunschweig.de

ABSTRACT

To successfully deal with a complex fouling problem usually entails a good understanding based on a broad spectrum of additional data. Meanwhile, a huge amount of process data is recorded and may be utilized to create a better understanding and prediction of the fouling status of an apparatus or the entire production plant.

We propose a systematic approach to generate training data in pipe fittings as a pre-step before the potential use of the entire data set of the production plant, irrespective of the relevance for the fouling prediction. Therefore, process parameter screening experiments as well as a temperature-based detection of the heat transfer resistance of plastic discs (representing 'artificial' fouling) and a particulate material deposition (representing 'real' fouling) were applied in pipe fittings obtaining reproducible results. The screening data exhibit linear as well as undefined fouling curves and are therefore very suitable for model training. The temperature measurements confirm a correlation between the obtained temperature drop and the layer thickness of the plastic discs as well as the deposited particles fouling mass.

INTRODUCTION

Fouling in production plants can quickly become a severe problem due to the omnipresence and complexity of the fouling mechanisms. Most processes experience not only one but a combination of the different fouling types [1]. Even though decades of research were spent in this area to describe the fouling mechanisms and postulate recommendations for countermeasures, still a large number of experiments are necessary to derive models or coherences in order to cope with a specific problem. It is easily becoming apparent that this approach is very time consuming and expensive.

It would therefore be a great advantage if more information could be drawn from the process itself to reduce the number of additional experiments necessary. Luckily, a large amount of process data is standardly recorded and archived during the operation of a production plant for documentation and traceability. These data were originally not

recorded to locate or predict fouling inside the plant but contain comprehensive information on the operational status of the plant and might also encapsulate relevant fouling-related information. Furthermore, sensors are widely used to record the most common process parameters such as temperature, pressure, volume flow, pH-value, conductivity etc., for online measurements. They are therefore inexpensive, easy to install and output an analogue or digital signal that can be directly processed and analyzed. Even though there might be a huge amount of data available, the sensors are measuring fouling either indirectly or locally. Hence, placing the sensor at positions which are representative for the fouling status of the entire plant presents the most challenging requirement in this context. This leads to the conclusion that an overall sensor concept is needed to make an improvement towards fouling prediction for the entire production plant with a simultaneous reduction of experiments needed.

The huge amount of data generated by such a sensor system which is ideally processed in real time for highly dynamic production processes requires powerful tools. With the help of Machine Learning (ML), which is a subfield of Artificial Intelligence (AI), it is possible to design systems that learn from input data and constantly improve the underlying models over time while being able to predict an outcome related to the given input data [2]. Since the field of progress engineering generates huge amounts of data, Data Science and ML are more and more applied for problems in production plants during the past years [3-4]. For example, an Artificial Neural Network generated a better result regarding fouling than the model proposed by the authors themselves [5]. Since there is already a lot of recent progress reported regarding the prediction of fouling inside important apparatuses with very specific properties like heat exchangers [6-8], this work focuses on pipe fittings as a group of plant components which are also susceptible to fouling while some are directly accessible to sensors. The measurements can then be used to draw conclusions about the fouling status of the apparatus (e.g., heat exchanger) in question.

As to the authors' knowledge, this aspect was not addressed in the literature so far as well as no systematic study has been carried out to comparatively characterize the fouling behavior of complex plant components with respect to a relevant sensor position to gain training data for fouling prediction. Instead of integrating the entire data set of a production plant irrespective of its relevance for the model prediction, a systematic approach to purposefully reduce the needed amount of data is proposed. Ultimately, the investigation aims towards the improved fouling prediction by the application of a reduced training data set. This is generated in a lab scale setup under defined process conditions while focusing on the fouling behavior of challenging scenarios regarding the deposition of soil. The experimental focus lay on the screening of prominent process parameters and the comparison of the different challenge scenarios. One fitting was investigated more closely to represent a group which is accessible for sensors to directly monitor fouling through the sensor signal. To provide the experimental basis for the detection, plastic discs (representing 'artificial' fouling) and a particulate material system (representing 'real' fouling) were applied. The thermal conductivity of the plastic discs used is in the same range as common fouling deposits [9] with the distinction that it is constant over the layer thickness and therefore represents an idealized fouling layer. A particulate substance system was chosen because the investigated pipe fittings highly influence the flow pattern which often creates areas of low flow velocity. These areas are very prone to particulate fouling which is mainly driven by sedimentation. Furthermore, the chemical inertness as well as flow behavior results in quite reproducible fouling layers which generates data that are highly applicable for model training. Nevertheless, particulate fouling is also a common problem in industry in forms of sand, dust or other particles [9]. Ultimately, the two systems were gauged directly by a temperature sensor in order to combine the results of the screening experiments with a sensor signal which can be directly processed and used for prediction in further work steps.

EXPERIMENTAL PROCEDURE

This section presents the experimental approach in order to generate the experimental training data by the systematic variation of process parameters as well as the pipe fittings with the application of soda-lime glass to generate particulate fouling layers. Furthermore, the methods to record the data for the detection of the artificial fouling layers (solid discs made of three different plastics and varying thickness) and the real (particulate) fouling layers via temperature measurements are presented.

Screening experiments for the generation of the training data

In order to evaluate the fouling behavior of pipe fittings with respect to a relevant sensor position for fouling prediction, comparative experiments were conducted. Soda-lime glass particles (Omicron solid glass beads NP3 P0 particles, Sovitec, Belgium) were used as a particulate model system for this work since it was already applied for previous studies [10-12] due to their advantageous substance properties such as being chemically inert, mono-disperse as well as relatively small (see Table 1).

Table 1: Properties of the particulate fouling system [10].

Parameter	Value
Density ρ_{part}	$2.5 \cdot 10^3 \text{ kg} \cdot \text{m}^{-3}$
Mean diameter $d_{part,50}$	$3.14 \text{ } \mu\text{m}$
Sphericity Ψ	≈ 1
Thermal conductivity λ	$1.0 \text{ W} \cdot \text{m}^{-1} \cdot \text{K}^{-1}$

Furthermore, it is supposed that ageing does not play an important role for particulate fouling which reduces the occurring mechanisms during fouling and therefore benefits the prediction accuracy [13]. Due to their low Stokes number ($St < 1$) it is assumed that the particles follow the fluid flow quite well and are therefore mainly driven by diffusion [14]. The particulate model system (Table 1) as well as the different pipe fittings (Table 2) were inserted into the test rig in deionized water (shown in Figure 1). The total suspension mass was set to 15 kg in order to highly exceed the amount of removed particles during the experiments. It was shown in pretests that a maximum of ca. 5 % (for the fittings exhibiting $d_{in} = 25 \text{ mm}$, 1 % on average for the fittings with $d_{in} = 6 \text{ mm}$ and $d_{in} = 10 \text{ mm}$, respectively) of the particles were extracted from the test rig as soil inside the pipe fittings for the parameter set which corresponds to the highest soil accumulation. Furthermore, it has to be taken into account that a certain mass of particles deposits in other parts of the test rig [15].

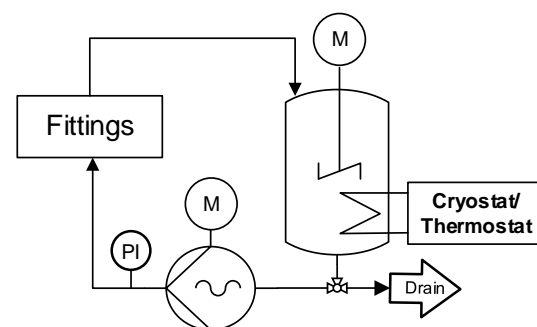


Figure 1: Process flow diagram of test rig I used for the screening experiments (fittings in Table 2) and temperature measurement (measurement fitting in Figure 2) with the particulate fouling system.

The test rig further consisted of a stirred tank (stirrer speed $n = 600 \text{ min}^{-1}$) which tempered the particle suspension to a constant temperature by a heating coil while providing high mixing to prevent particle sedimentation. The suspension was drawn from the storage tank by an eccentric screw pump which circulated the fluid through a pipe system consisting of the calming section, the pipe fitting of interest, the outlet section and the reflux into the storage tank. A pressure sensor was installed directly downstream of the pump to monitor the resulting pressure drop, but was not evaluated in this study.







In order to compare experiments with regards to the resulting fouling mass, the dimensionless Reynolds number was kept constant. The Reynolds number is widely used to characterize the flow pattern with respect to its turbulence and is calculated applying Eq. (1) whereas ρ_{fl} and η_{fl} are the temperature-dependent density and dynamic viscosity of the fluid, respectively. The differences between the physical properties for the particle suspension (see Table 1) and water are considered negligible ($< 1 \%$), therefore the calculations were performed with the properties of water [9]. The pipe diameter d_{in} as well as the average flow velocity \bar{u} are dependent on the applied dimension and volume flow, respectively.

$$Re = \frac{\rho_{fl} \cdot d_{in} \cdot \bar{u}}{\eta_{fl}} \quad (1)$$

To provide a fully developed turbulent flow pattern upstream of the pipe fitting, a calming section L_c was provided ($30 \cdot d_{in}$) [16]. The outlet section was determined to half the length of the calming section. In order to systematically generate training data with fittings, a pipe socket, bend socket, pipe bend, nozzle, diffuser and a valve were investigated (see Table 2). For direct comparison, all fittings were purchased from the same manufacturer (Hy-Lok CO., LTD., Republic of Korea) and made of the same material SS316. In preparation of all experiments, the fittings were cleaned with lab soap (PBS®T 105, Carl Roth GmbH + Co. KG, Germany) in water, degreased by $0.7 \text{ L} \cdot \text{L}^{-1}$ Ethanol, treated in an ultrasonic bath in $0.25 \text{ mol} \cdot \text{L}^{-1}$ Citric acid for 10 min and finally rinsed with deionized water.

The screening experiments were conducted with varying process parameters for the different pipe fittings. The parameter range is shown in Table 3. After each experiment the corresponding fitting was dismantled, the supernatant liquid of the remaining particle suspension removed and the fitting dried over night for at least $t = 12 \text{ h}$ at $\vartheta = 60 \text{ }^\circ\text{C}$. The obtained fouling mass was referred to the total inner surface area of the corresponding fitting (see Table 2) in order to calculate the specific fouling mass m_f .

Table 2: Properties of the investigated pipe fittings. The pipe sockets with a pipe diameter of $d_{in} = 6 \text{ mm}$ and $d_{in} = 10 \text{ mm}$ exhibited an $L_{\text{pipe}} \cdot d_{\text{pipe}}^{-1} = 10$ ratio, the sockets with $d_{in} = 25 \text{ mm}$ an $L_{\text{pipe}} \cdot d_{\text{pipe}}^{-1} = 5$ ratio. Direction of flow from right to left and upwards, respectively.

Symbol	Name	Inner diameter d_{in} / mm	Inner surface area A_{in} / m^2
	Pipe socket	6	$1.2 \cdot 10^{-3}$
		10	$3.2 \cdot 10^{-3}$
		25	$1.0 \cdot 10^{-2}$
	Pipe Bend	6.3	$5.0 \cdot 10^{-4}$
	Bend socket	6	$1.2 \cdot 10^{-3}$
	Nozzle	7.9/6.3	$2.3 \cdot 10^{-4}$
	Diffuser	6.3/7.9	$2.3 \cdot 10^{-4}$
	Valve	6.3	$4.1 \cdot 10^{-4}$

Since a pipe socket is a widely used fitting for the installation of sensors, the screening experiments were mostly performed applying this component. Furthermore, the pipe bend, which is a fitting that is not accessible directly by a sensor, was also further investigated in order to provide the basis for an indirect prediction of its fouling status during further work, that is not in the focus of this paper.

Table 3: Parameter range for the screening experiments with the particulate fouling system.

Parameter	Min.	Max.
Particle mass fraction $w / \frac{g_{\text{part}}}{g_{\text{tot}}}$	0.005	0.03
Average flow velocity $\bar{u} / \frac{\text{m}}{\text{s}}$	1.12	4.42
Time t / min	1	360
Temperature $\vartheta / \text{ }^\circ\text{C}$	20	50

Temperature measurements for the direct detection of artificial and real fouling layers

To be able to combine the training data obtained for the pipe fittings by gravimetric measurement of the deposited particles with a processible sensor signal, the focus of these measurements lay exclusively on the pipe socket with $d_{in} = 25 \text{ mm}$. Furthermore, the approach was divided into two steps.

Firstly, artificial fouling layers made of plastic discs with a diameter of $d_{in} = 25 \text{ mm}$ were inserted into the measuring socket shown in Figure 2 (red area) which was then included into test rig II shown in

Figure 3. Afterwards, the temperature sensor was used to characterize the system with regards to a varying thermal conductivity and layer thickness of the plastic discs.

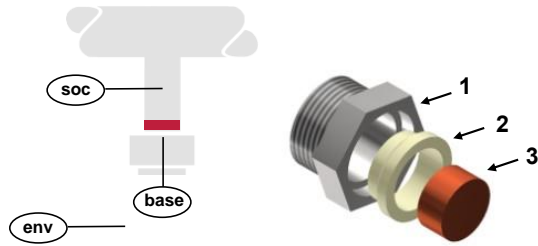


Figure 2: Schematic illustration of the measuring fitting and the position of the three temperature sensors: socket medium (soc), base plate (base), environment (env) (left) and an explosion drawing showing the stainless-steel screw (1), the insulation ring (2) and the copper bottom plate (3) (right).

Secondly, particulate fouling experiments were performed with the same measuring socket (Figure 2) but this time included into test rig I (see Figure 1) because only this test rig is suitable for experiments with particles. Here, the temperature was measured online to detect an alteration in the signal with regards to an increasing particulate fouling layer. The base plate is made of copper (Cu-ETP, EW004A, Hans-Erich Gemmel & Co. GmbH, Germany) to ensure an optimal distribution of the heat transferred from the medium towards the inner base surface. A polypropylene (PP-H natur, Max Wirth GmbH, Germany) ring ensures thermal insulation so that the heating of the copper plate is only induced by the heat flux from the suspension medium and not from heat conduction by a direct connection to the metal pipe. Three resistance thermometers (PT1000 Einschraub-Widerstandsthermometer class AA, Therma Thermofühler GmbH, Germany) were used to measure the temperature inside the suspension socket medium (soc), inside the copper base plate (base) and the ambient air temperature (environment) right next to the pipe socket. The pipe was insulated with insulation wool except for the copper base plate to ensure the heat flux from the suspension medium through the copper block towards the surrounding air. The measuring socket was inserted into test rig II shown in Figure 3 for the experiments regarding the artificial fouling layers. This rig exceeds test rig I shown in Figure 1 in applicable volume flow and temperature range.

The process medium was preheated and constantly stirred in one of the storage tanks while it was pumped through the measuring section beforehand to ensure a constant temperature of the pipes. For the start of the experiment, a blind socket was replaced with the measuring socket before the recording was started. The experiments were conducted as stated in Table 4. The temperature dependency of the thermal

conductivity of solids is not very distinctive in a small range and can be neglected [17].

Table 4: Parameters for the experiments with the artificial fouling layers applied inside test rig II, displayed in Figure 3.

Parameter	Value
Average pipe flow velocity	0.72 m·s ⁻¹
Storage tank temperature	50 °C
Medium	Water
Medium volume	50 L

Therefore, the values for the thermal conductivity given for $\vartheta = 20$ °C by the manufacturer, shown in Table 5, can be used for the experiments performed at $\vartheta = 50$ °C. The stated disc layer thickness is the actually measured thickness which differs between the plastics due to production tolerances. The temperature drop which results through the setup presented in Figure 3 is recorded for every test series without plastic layers to determine the offset. To record the heating phase the sensor was tempered to 20 °C before it was inserted into the test rig.

Table 5: Properties of the investigated artificial fouling layers at $\vartheta = 20$ °C.

Material	PVC-U	PA-6	PE-HD
Thermal conductivity λ / W·m ⁻¹ ·K ⁻¹	0.16	0.23	0.42
Disc layer thickness δ / mm	1	1	1
	2	2	2
	3	2.9	3.1
	4	3.9	4.2
	4.9	4.9	5
	8	8	8

The end values of the recorded temperature curves were recorded for the ‘clean’ socket to determine the temperature offset due to the heat transfer limitation of the setup as indicated in Eq. (2).

$$\Delta T_{off} = \vartheta_{soc} - \vartheta_{base} \quad (2)$$

The offset can now be subtracted from the obtained temperatures of the socket medium and the sensor at the base of the socket with the plastic cylinders added (see Eq. (3)).

$$\Delta T = \vartheta_{soc} - \vartheta_{base,f} - \Delta T_{off} \quad (3)$$

To perform the temperature measurements with the particulate substance system, the measuring socket (Figure 2) was inserted into test rig I for the screening experiments (see Figure 1). The preparation and conduction were performed in the same way as for the screening experiments while the

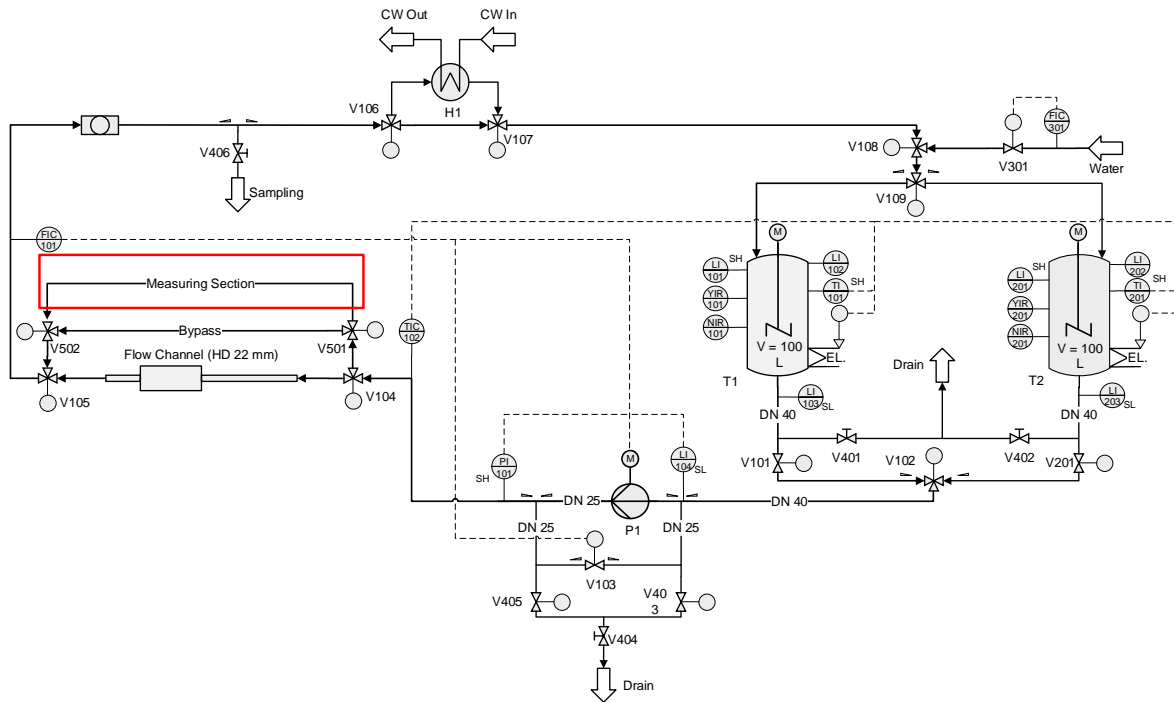


Figure 3: Process flow diagram of test rig II for the trails with artificial fouling layers inside the pipe socket with temperature sensors.

temperature signals were recorded online by a data logger (Agilent 34970A, Keysight Technologies, Inc., USA). The only difference refers to the applied particle mass fraction. While the screening experiments were performed with a maximum particle mass fraction of $w = 0.03 \text{ g}_{\text{part}} \cdot \text{g}_{\text{tot}}^{-1}$, a higher value of $w = 0.05 \text{ g}_{\text{part}} \cdot \text{g}_{\text{tot}}^{-1}$ was set for the temperature measurements of the particulate fouling to be sure to have enough particles for a noticeable fouling detection.

RESULTS

This section presents the experimental results that were generated for the training data set. Firstly, the influence of process parameters and fitting type variation on the resulting fouling mass were investigated (test rig I, see Figure 1). Secondly, the influence of artificial fouling in the measuring fitting (see Figure 2) in test rig II (see Figure 3) as well as real fouling layers in the measuring fitting (see Figure 2) in test rig I (see Figure 1) on the signal of a temperature sensor inside a pipe socket were investigated to monitor the obtained signal over time.

Process parameter screening

In order to generate training data for improved fouling prediction, typical parameters known to influence the given process and therefore the fouling result were investigated. Since problems regarding particulate fouling are well known in applications dealing with sand, mud or corrosion products, the actual particle mass fraction is often not known [15]. Therefore, Figure 4 presents results of a systematic variation of the mass fraction. The specific fouling

mass increases linearly with higher particle mass fraction ($R^2 = 0.98$) in the investigated parameter range. Generally, it was shown in previous works that the particle concentration has the greatest influence on the resulting fouling [11,18]. In literature, the problem of particulate fouling is mostly addressed in heat exchangers and asymptotic or falling rate curves are observed with variation of the particle concentration. Since the investigated parameter range in this work is quite narrow ($0.005 \text{ g}_{\text{part}} \cdot \text{g}_{\text{tot}}^{-1} \leq w \leq 0.03 \text{ g}_{\text{part}} \cdot \text{g}_{\text{tot}}^{-1}$), a change in the progression of the curve for higher particle mass fractions is expected. The different application, substance systems as well as varying process parameters makes a direct comparison with the literature quite challenging.

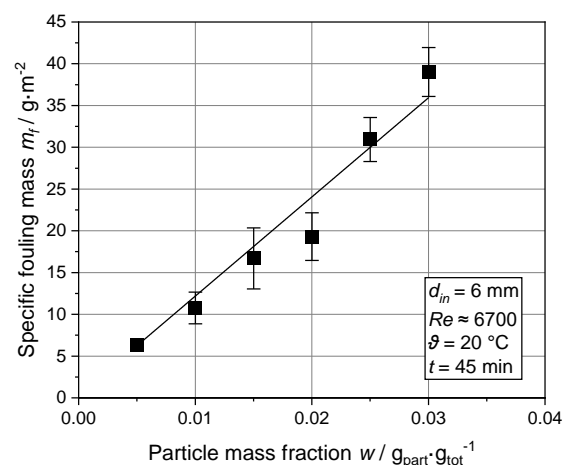


Figure 4: Influence of the particle mass fraction on the obtained specific fouling mass for the pipe socket.

In this work, the obtained soil monitored in the pipe fittings is mainly driven by sedimentation due to a decrease in the fluid velocity caused by the fitting

geometry. Specially the pipe socket leads to chaotic vortices inside the dead zones and therefore to a decrease in fluid velocity [19-20].

The average fluid velocity is another commonly addressed parameter with regards to the fouling result. Figure 5 displays the obtained specific fouling mass of the pipe socket for the parameter range of $1.12 \text{ m}\cdot\text{s}^{-1} \leq \bar{u} \leq 4.42 \text{ m}\cdot\text{s}^{-1}$. It is obvious that the data set can be divided into two sections. Below a velocity of $3.33 \text{ m}\cdot\text{s}^{-1}$ the parameter adjustment does not influence the resulting soil mass. In contrast, the soil mass rises strongly above this threshold. Previous works report that, in general, an increase of fluid velocity leads to a reduction of fouling. This is due to the increased shear stress that on one hand reduces the deposition of e.g., particulate systems. On the other hand, local overheating increases fouling rates for e.g., crystallization or polymer fouling. This especially occurs in dead zones or grooves which favor the deposition of the foulant because they provide protection from the influence of the fluid flow [1,5,19]. The observed increase of deposition in this work cannot be compared directly with the findings in the literature since the geometry of the pipe socket leads to a complex fluid flow. Studies show that the flow velocity decreases strongly with an increase of the dead space [20]. It is therefore assumed that a variation of the average flow velocity in the main pipe only has a minor effect on the deposition inside the dead end since the flow velocity is greatly reduced therein. The observed increase of foulant in Figure 5 can rather be explained by a higher particle supply due to the enlarged volume flow that corresponds to the flow velocity while the experiment runtime was kept constant.

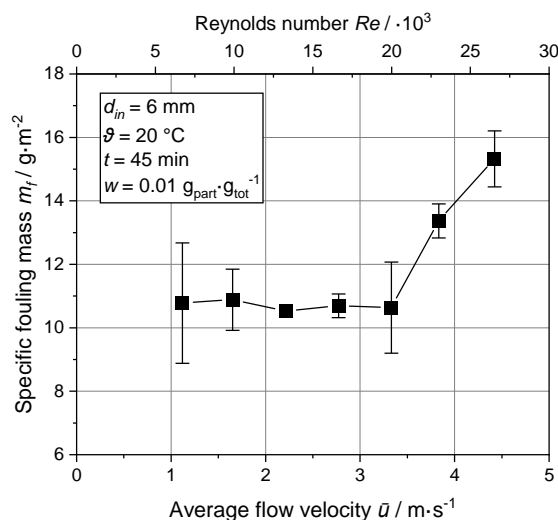


Figure 5: Obtained specific fouling mass for the pipe socket with respect to varying average flow velocity and Reynolds number, respectively.

The fluid temperature and process runtime are two further known factors to influence the fouling result. As plotted in Figure 6, a longer experiment runtime

leads to an increase of the fouling mass for the investigated temperatures. Due to pumping limitations of the setup the experiments for the temperature variation were carried out with fittings exhibiting $d_{in} = 10 \text{ mm}$.

The increase is found to be linear for a temperature of $\vartheta = 20 \text{ }^\circ\text{C}$ ($R^2 = 0.95$) as well as $\vartheta = 35 \text{ }^\circ\text{C}$ ($R^2 = 0.98$) in the investigated parameter range, while the curve for $\vartheta = 50 \text{ }^\circ\text{C}$ does not seem to follow a known course. A further step will be the increase of the experiment runtime to determine if the deposition and the removal of soil repeats over time and can therefore be described by sawtooth behavior. Interestingly, the curve of the obtained data points for runtimes below $t = 30 \text{ min}$ does not differ much from the data for $\vartheta = 20 \text{ }^\circ\text{C}$ and $\vartheta = 35 \text{ }^\circ\text{C}$, respectively. The data at $t \geq 30 \text{ min}$ exhibit a high deviation between the replicates and lower fouling masses. The high deviation supports the assumption of a sawtooth behavior because of the poor chance of reproducibility. Even though the volume flow for the experiments at $\vartheta = 50 \text{ }^\circ\text{C}$ is reduced compared to $\vartheta = 20 \text{ }^\circ\text{C}$ in order to result in the same Reynolds number (dynamic viscosity is reduced by ca. 45 % when heating from $20 \text{ }^\circ\text{C}$ to $50 \text{ }^\circ\text{C}$), a higher removal rate at certain time points seems to occur which leads to the observed course of the graph.

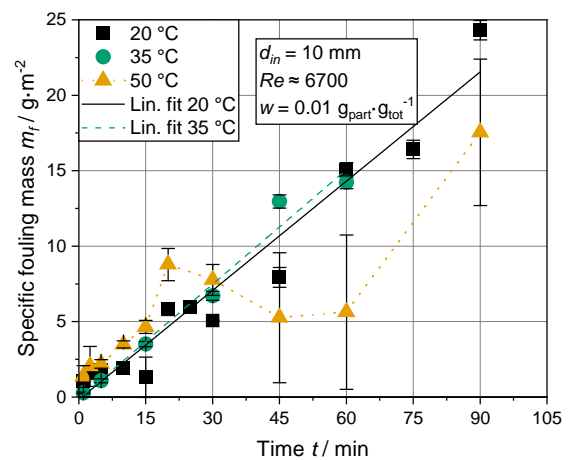


Figure 6: Progression of the specific fouling mass over time with respect to the temperature for the pipe socket.

Variation of the fitting geometry

It was already mentioned above that the geometry has a huge influence on the fouling result. Therefore, a direct comparison between six common pipe fittings was performed under constant conditions (see Figure 7). It is not surprising with regards to its complex geometry that the valve exhibits by far the highest specific fouling mass. Furthermore, even though the pipe socket and bend socket share the same basic geometry, the bend socket is affected a lot less by particle deposition. The chosen pipe socket and pipe bend exhibit similar fouling for the

set parameter range. Since the basic idea of the introduced concept for the application of training data for improved fouling prediction includes a transfer from a measuring towards a target fitting, these two ubiquitous and easily scalable fittings were chosen for further detailed investigation. For direct comparison, Figure 8 shows the development of the specific fouling mass over time for the pipe socket and pipe bend for $d_{in,socket} = 6$ mm and $d_{in,bend} = 6.3$ mm, respectively.

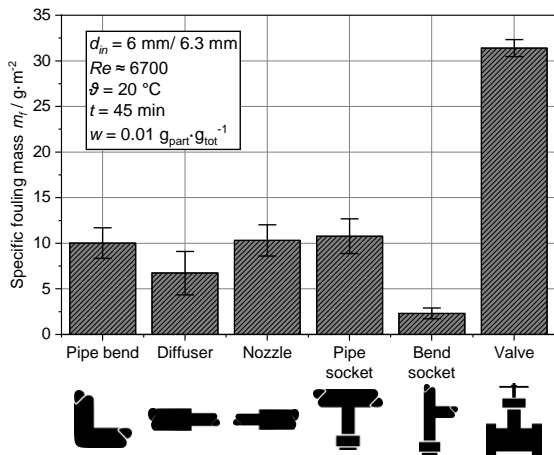


Figure 7: Direct comparison of the obtained specific fouling mass of all investigated pipe fittings.

Like the data shown in Figure 6 for the pipe socket at $\vartheta = 20$ °C and $d_{in} = 10$ mm, the fouling mass increases linearly over time. The pipe bend exhibits a presumed sawtooth behavior which corresponds with the much higher shear stress inside the fitting due to a direct exposure and the lack of death space. Interestingly, in contrast to the data of the pipe socket, the pipe bend already shows a comparably high fouling mass for very low runtimes which is not exceeded that much over the observed range.

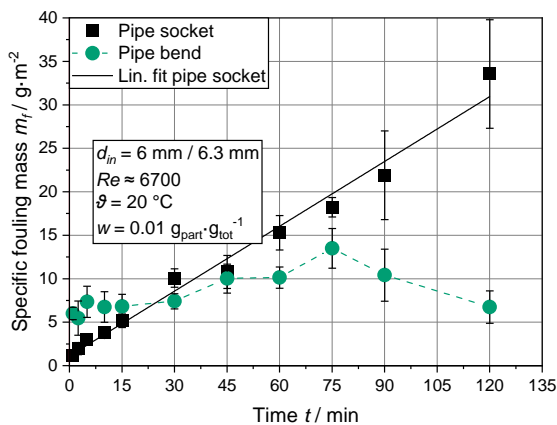


Figure 8: Progression of the specific fouling mass over time for the pipe socket and pipe bend.

It is likely that the observed fouling layer develops directly after the start of the experiment to a certain point and is quickly limited due to the high shear stress in the fitting. Even though the fouling mass

per area is similar between the pipe socket and the pipe bend, the inner surface area of the bend is only 43 % compared to the area of the pipe socket resulting in a difference between the total fouling mass. A direct comparison of two pipe sockets with a different size is illustrated in Figure 9, showing that the fouling mass per inner surface area increases linearly and does not differ much between the $d_{in} = 6$ mm ($R^2 = 0.98$) and the $d_{in} = 10$ mm ($R^2 = 0.95$) fouling curve at $\vartheta = 20$ °C.

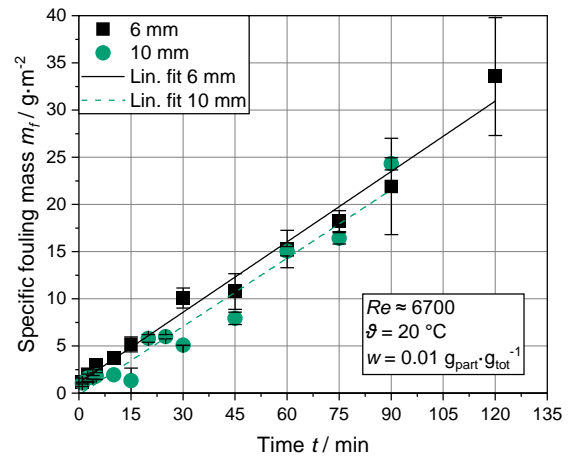


Figure 9: Progression of the specific fouling mass over runtime with respect to the inner pipe diameter of the pipe socket at $\vartheta = 20$ °C.

The comparison between the inner diameter looks different for the parameters compared in Figure 10. Here, the start of a sawtooth behavior is assumed for both diameters investigated. It is noteworthy that the first large removal of fouling mass seems to be shifted to a higher runtime ($30 \text{ min} \leq t \leq 45 \text{ min}$) for the larger diameter compared to the smaller one ($20 \text{ min} \leq t \leq 30 \text{ min}$).

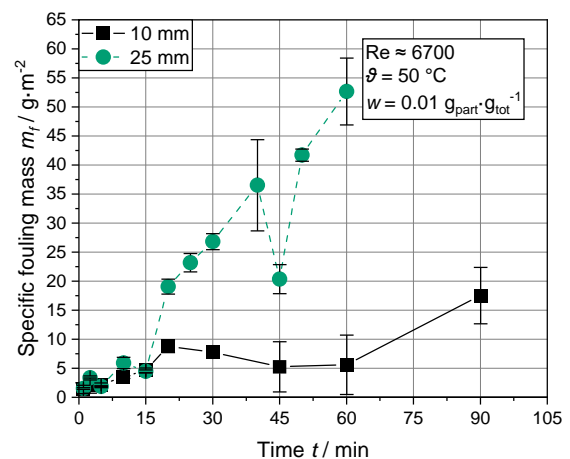


Figure 10: Progression of the specific fouling mass over runtime with respect to the inner pipe diameter of the pipe socket at $\vartheta = 50$ °C.

Temperature measurements with artificial fouling layers

Since the gravimetric determination of the fouling mass inside the fittings presented in the previous section is not practical for industrial processes, a direct fouling detection by a sensor signal is proposed. In a first step, artificial fouling layers (discs with $d_{in} = 25$ mm) made of three different plastics are inserted into the measuring fitting (Figure 2) which was mounted to test rig II (Figure 3) since the layer thickness and thermal conductivity of the plastics is constant and known precisely. An example for the temperature curve progression is shown in Figure 11 for the offset measurement. It is visible that the measuring fitting takes ca. $t = 15$ min to adjust to a constant temperature of approx. $\vartheta = 46.7$ °C even though the medium temperature in the pipe socket is $\vartheta = 49.1$ °C on average. Once the artificial fouling layer discs are inserted and the experiments run until a constant sensor temperature, a temperature drop is observed between the blank sensor and the installation of the plastic discs. The results are used to calculate the data presented in Figure 12 by applying Eq. 2 and Eq. 3.

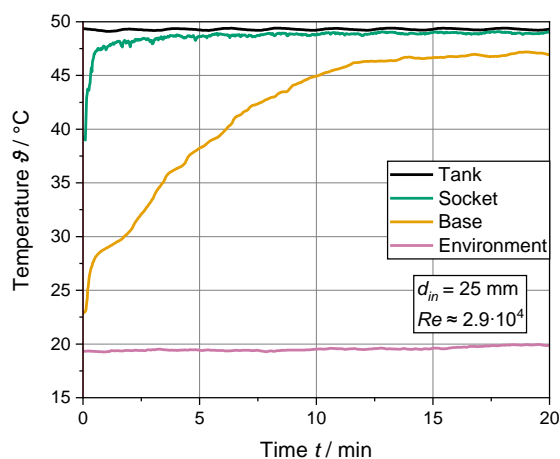


Figure 11: Temperature signals over the experiment runtime for the offset measurement.

It is visible that the layer thickness has the strongest influence on the resulting temperature drop. The increase of the temperature drop is not proportional as expected by Fourier's law. This can be explained because for higher values of layer thickness the conditions for the application of Fourier's law are not provided: The diameter of the plastic discs is no longer extended infinitely with regards to the layer thickness [9]. A plate inside a pipe socket differs a lot from two parallel walls as defined in the model assumption. Unlike the model assumption, the heat flow is not exclusively directed orthogonally through the plastic disc. Since the disc is also surrounded by the metal pipe a heat flow from the sides increases the heat flux from the fluid medium.

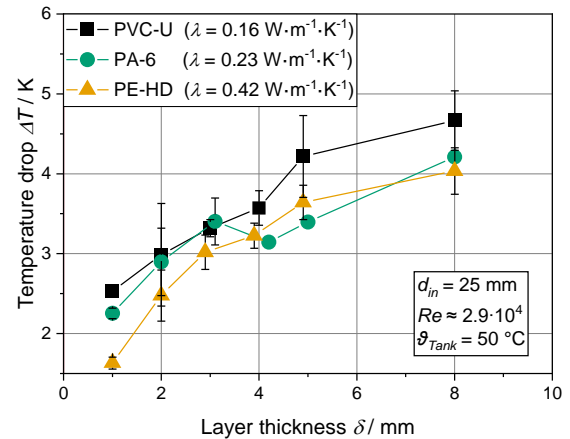


Figure 12: Obtained temperature difference between the medium temperature and the base plate sensor corrected by the offset for PVC-U, PA-6 and PE-HD.

Therefore, especially valid for the plastic cylinders exhibiting a greater layer thickness, the influence of the heat transfer from the side of the cylinder through the pipe wall cannot be neglected. The variation of the plastic type results in a distinguishable temperature drop for a low layer thickness ($\delta \leq 2$ mm). Here, the expected trend is observed that a lower thermal conductivity leads to a higher temperature drop. Above the threshold of $\delta = 2$ mm the trend is not visible anymore. Since not all data points are backed up by at least three replicates yet, further experiments need to be conducted.

Temperature measurements with particulate fouling layers

After the confirmation of the general suitability of the measuring setup for a temperature drop which is dependent on the plastic disc layer thickness, in this section the results of the online fouling experiments with the soda-lime glass particles are presented. Therefore, the measuring fitting shown in Figure 2 was inserted into test rig I, shown in Figure 1. Figure 13 presents the signal course of the temperature sensors positioned in the pipe socket, in the socket base and in the environment next to the socket. The environment temperature fluctuates and increases slightly over the experiment runtime similarly to the offset measurements (Figure 11) due to draughts and heating up in the laboratory but does not seem to influence the other signals directly. The signal of the base sensor differs compared to the signal of the offset measurements (Figure 11). It is visible that the signal of the base sensor changes over time even though the socket temperature stays constant. To investigate the signal of the base sensor more closely, Figure 14 shows a magnification of that data set. In contrast to the offset experiments shown in Figure 11 the base sensor was preheated and therefore does not show a heat-up phase. This

initial temperature drop is due to the preheating of the sensor. The base sensor is preheated externally to a temperature of $\vartheta = 47\text{ °C}$ in order to skip a heating up from room temperature. This temperature slightly above the resulting temperature during the experiment was chosen because the sensor cools down faster than it heats up. After the temperature adjustment the curve exhibits a local minimum.

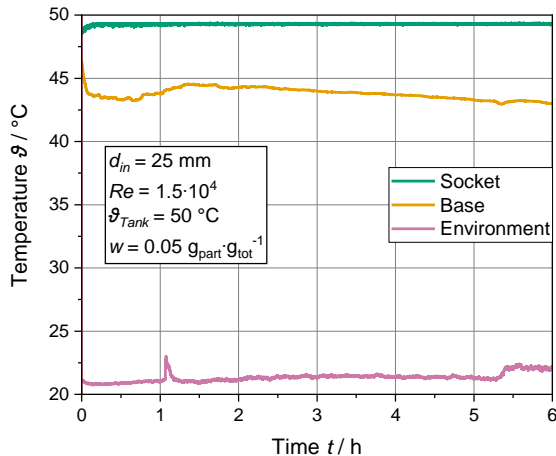


Figure 13: Temperature course of the sensors for the online particulate fouling measurement.

Since the signal also shows a high noise, it is assumed that, due to the chaotic fluid flow inside the pipe socket, partly a fluidized bed is formed and overlays the initial buildup of the particulate fouling layer. After a strong increase of the temperature towards a maximum of 44.5 °C at ca. 1.35 h, the signal decreases linearly ($R^2 = 0.98$) exhibiting a lot less noise than for $t \leq 1.35\text{ h}$. To confirm the reproducibility of this finding, three replicates were conducted in total to derive the final specific fouling mass and the dynamic temperature drop (see Figure 15).

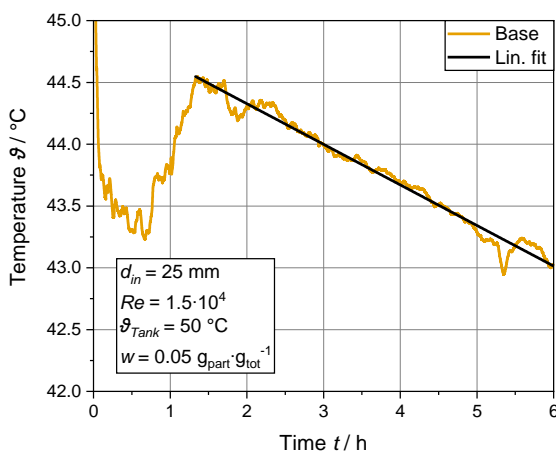


Figure 14: Zoom of temperature course of the sensor for the online particulate fouling measurement.

It is visible that the deviation between the experiments is quite low since the signal follows a

linear relation (for the given parameter set, after the initiation phase). This is a good basis for the use as training data since no complex models are needed. The obtained specific fouling mass increased a hundredfold compared with the results of the screening experiments shown in Figure 4 for the chosen parameter range. This is mainly driven by the higher particle mass fraction and long runtime. In order to have more reliable training data, the parameter range for the screening results should be extended towards the range set for the temperature measurements.

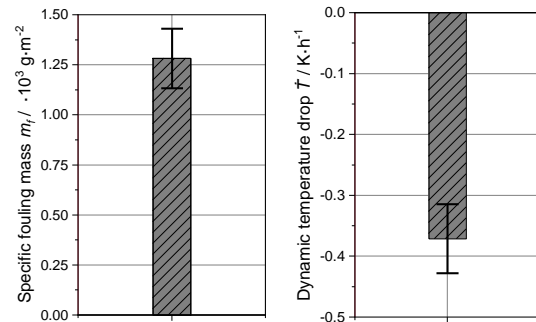


Figure 15: Specific fouling mass (left) and the dynamic temperature drop (right) after six hours of experiment runtime for the particulate fouling measurements.

CONCLUSION

A systematic approach for the generation of training data for improved fouling prediction in pipe fittings was presented by the application of a particulate fouling system. The variation of process parameters and pipe fitting geometry demonstrate that it is possible to generate reproducible data that obtain different correlations regarding the obtained specific fouling mass and are therefore very suitable for model training.

The results obtained with the artificial fouling layers confirm that they serve as an insulation layer between the fluid inside the socket and the sensor resulting in a measurable temperature drop. Furthermore, a dependency between the fouling layer thickness and the temperature drop can be recorded. A difference between the plastic materials is not very pronounced due to the narrow range of the corresponding values for thermal conductivity.

When the artificial fouling layers are replaced by the particulate fouling system, the results show that the buildup of a particulate fouling layer can also be measured directly online by the temperature signal. The obtained dynamic temperature drop from the linear decrease of the signal as well as the final obtained specific fouling mass are reproducible and fit into the observations of the screening experiments for the pipe fittings. Furthermore, a fluidized bed occurs presumably during the initiation phase of the experiment and should be

further investigated with respect to the detection by the temperature signal directly.

Ongoing work is extending the screening experiments of fouling in the pipe fittings in order to better understand the correlations between the parameters described above. Furthermore, more replicates will be conducted to increase the validity of the measurements regarding the artificial fouling layers. A parameter variation as well as a time series forecasting is going to be performed for the temperature measurements with the particulate system. Ultimately, the results will be combined to convert the forecasting of the signal at the measuring fitting towards the target fitting.

ACKNOWLEDGEMENTS

The authors thank the mechanical and electrical workshop of the ICTV for their support with the buildup of the test rigs. The conduction of the experiments by Julia Buschermöhle, Xuyang Feng, Renan Louro Cardoso Franco, Leon Paul, Olinda Sidorow and Elisabeth Tartler is greatly appreciated.

NOMENCLATURE

Abbreviations

AI	Artificial Intelligence
ML	Machine Learning
PA-6	Polyamid 6
PE-HD	Polyethylene high density
PVC-U	Unplasticized Polyvinylchloride

Latin letters

A	Area, m^2
c_p	Specific heat capacity, $J \cdot g^{-1} \cdot K^{-1}$
d	Diameter, mm
L	Length, m
m	Mass, g
m_f	Specific fouling mass, $g \cdot m^{-2}$
n	Tank stirrer speed, min^{-1}
t	Time, min
R^2	Coefficient of determination, -
Re	Reynolds number, -
St	Stokes number, -
T	Absolute temperature, K
\dot{T}	Dynamic temperature drop, $K \cdot h^{-1}$
\bar{u}	Average flow velocity, $m \cdot s^{-1}$
w	Particle mass fraction, $g_{part} : g_{tot}^{-1}$

Greek letters

δ	Layer thickness, mm
Δ	Difference, -
η	Dynamic viscosity, $kg \cdot m^{-1} \cdot s^{-1}$
λ	Thermal conductivity, $W \cdot m^{-1} \cdot K^{-1}$
ρ	Density, $kg \cdot m^{-3}$
ϑ	Temperature, $^{\circ}C$
Ψ	Sphericity, -

Subscript

<i>base</i>	sensor position at socket base
<i>bend</i>	pipe bend

<i>c</i>	calming
<i>env</i>	environment
<i>f</i>	fouling
<i>fl</i>	fluid
<i>in</i>	inner
<i>loss</i>	deposited particles in the test rig
<i>m</i>	medium
<i>off</i>	offset
<i>part,50</i>	mean particle value
<i>part</i>	particle
<i>pipe</i>	corresponding pipe
<i>sen</i>	sensor
<i>soc</i>	sensor position in the socket medium
<i>socket</i>	pipe socket
<i>tank</i>	storage tank
<i>tot</i>	total

REFERENCES

- [1] N. Epstein, Thinking about heat transfer fouling: A 5×5 matrix, *Heat Transfer Engineering*. 4 (1983) 43–56. <https://doi.org/10.1080/01457638108939594>.
- [2] J. Bell, *Machine Learning: Hands-on for Developers and Technical Professionals*, 1. Edition, Wiley, Indianapolis (2014). <https://books.google.de/books?id=YP-7nQAACAAJ>.
- [3] L. Chiang, B. Lu, I. Castillo, Big Data Analytics in Chemical Engineering, *Annual Review of Chemical and Biomolecular Engineering*. 8 (2017) 63–85. <https://doi.org/10.1146/annurev-chembioeng-060816-101555>.
- [4] Z. Ge, Z. Song, S.X. Ding, B. Huang, Data Mining and Analytics in the Process Industry: The Role of Machine Learning, *IEEE Access*. 5 (2017) 20590–20616. <https://doi.org/10.1109/ACCESS.2017.2756872>.
- [5] H. Müller-Steinhagen, Heat transfer fouling: 50 years after the Kern and Seaton model, *Heat Transfer Engineering*. 32 (2011) 1–13. <https://doi.org/10.1080/01457632.2010.505127>.
- [6] S. Sundar, M.C. Rajagopal, H. Zhao, G. Kuntumalla, Y. Meng, H.C. Chang, C. Shao, P. Ferreira, N. Miljkovic, S. Sinha, S. Salapaka, Fouling modeling and prediction approach for heat exchangers using deep learning, *International Journal of Heat and Mass Transfer*. 159 (2020). <https://doi.org/10.1016/j.ijheatmasstransfer.2020.120112>.
- [7] S. Uguz, O. Ipek, Prediction of the parameters affecting the performance of compact heat exchangers with an innovative design using machine learning techniques, *Journal of Intelligent Manufacturing*. (2021). <https://doi.org/10.1007/s10845-020-01729-0>.

- [8] E.M.S. El-Said, M. Abd Elaziz, A.H. Elsheikh, Machine learning algorithms for improving the prediction of air injection effect on the thermohydraulic performance of shell and tube heat exchanger, *Applied Thermal Engineering*. 185 (2021) 116471.
- [9] Gesellschaft VDI, VDI-Wärmeatlas, 11. Auflage, Springer Berlin Heidelberg, Wiesbaden (2013).
- [10] R. Kasper, H. Deponte, A. Michel, J. Turnow, W. Augustin, S. Scholl, N. Kornev, Numerical investigation of the interaction between local flow structures and particulate fouling on structured heat transfer surfaces, *International Journal of Heat and Fluid Flow*. 71 (2018) 68–79.
<https://doi.org/10.1016/j.ijheatfluidflow.2018.03.002>.
- [11] H. Deponte, L. Rohwer, W. Augustin, S. Scholl, Investigation of deposition and self-cleaning mechanism during particulate fouling on dimpled surfaces, *Heat and Mass Transfer*. 55 (2019) 3633–3644.
<https://doi.org/10.1007/s00231-019-02676-0>.
- [12] H. Deponte, R. Kasper, S. Schulte, W. Augustin, J. Turnow, N. Kornev, S. Scholl, Experimental and numerical approach to resolve particle deposition on dimpled heat transfer surfaces locally and temporally, *Chemical Engineering Science*. 227 (2020).
<https://doi.org/10.1016/j.ces.2020.115840>.
- [13] D. Wilson, E. Ishiyama, W.R. Paterson, A.P. Watkinson, Ageing: Looking back and looking forward, *Proceedings of International Conference on Heat Exchanger Fouling and Cleaning VIII*. 2009, Schladming (2009) 221–230.
- [14] H. Deponte, Lokales Partikelfouling auf wärmeübertragenden Dellenoberflächen, Dissertation Technische Universität Braunschweig (2021).
- [15] R. Blöchl, H. Müller-Steinhagen, Influence of particle size and particle/fluid combination on particulate fouling in heat exchangers, *The Canadian Journal of Chemical Engineering*. 68 (1990) 585–591.
<https://doi.org/10.1002/cjce.5450680408>.
- [16] H. Sigloch, Technische Fluidmechanik, 10. Auflage, Springer Vieweg, Heidelberg (2017).
<https://doi.org/10.1007/978-3-662-54467-9>.
- [17] H.D. Baehr, K. Stephan, Wärme- und Stoffübertragung, 9. Auflage, Springer Vieweg, Heidelberg (2016).
- [18] H. Müller-Steinhagen, F. Reif, N. Epstein, A.P. Watkinson, Particulate fouling during boiling and non-boiling heat transfer, *Proceedings 8th Int. Heat Transfer Conference* 5, 2555, San Francisco 26 (1986).
- [19] A. Grasshoff, Hygienic Design - The basis for computer controlled automation, *Proceedings IChemE Conference “Food Engineering in a Computer Climate.”* 70 (1992).
- [20] E. Deutsch, N. Mechtoua, J.D. Mattei, Flow simulation in piping system dead legs using second moment, closure and k-epsilon model, (EDF--96-NB-00180) France (1996).
http://inis.iaea.org/search/search.aspx?orig_q=RN:28064447.